

Towards Safe Autonomous Driving: A Real-Time Motion Planning Algorithm on Embedded Hardware

Korbinian Moller, Glenn Johannes Tungka, Lucas Jürgens, Johannes Betz

Abstract—Ensuring the functional safety of Autonomous Vehicles (AVs) requires motion planning modules that not only operate within strict real-time constraints but also maintain controllability in case of system faults. Existing safeguarding concepts, such as Online Verification (OV), provide safety layers that detect infeasible planning outputs. However, they lack an active mechanism to ensure safe operation in the event that the main planner fails. This paper presents a first step toward an active safety extension for fail-operational Autonomous Driving (AD). We deploy a lightweight sampling-based trajectory planner on an automotive-grade, embedded platform running a Real-Time Operating System (RTOS). The planner continuously computes trajectories under constrained computational resources, forming the foundation for future emergency planning architectures. Experimental results demonstrate deterministic timing behavior with bounded latency and minimal jitter, validating the feasibility of trajectory planning on safety-certifiable hardware. The study highlights both the potential and the remaining challenges of integrating active fallback mechanisms as an integral part of next-generation safeguarding frameworks. The code is available at: <https://github.com/TUM-AVS/real-time-motion-planning>

I. INTRODUCTION

Over the last few years, Autonomous Vehicles (AVs) have gained significant attention due to their potential to enhance traffic efficiency and accessibility [1]. Furthermore, by reducing human error, the predominant cause of traffic accidents, AVs promise to significantly lower crash rates.

Despite these advantages, the deployment of AVs in complex environments remains a challenge. Motion planning, in particular, is a safety-critical component that must operate under strict timing and memory constraints [2]. If trajectory computation exceeds its deadline or produces infeasible outputs, vehicle controllability can no longer be guaranteed. To mitigate this risk, several research efforts have focused on Online Verification (OV) and runtime safeguarding, where an independent module continuously checks the feasibility and timing of planning outputs [3], [4]. These approaches enable ASIL decomposition in accordance with ISO 26262 [5], allowing a safety layer to supervise complex, nondeterministic planners. However, these mechanisms often remain passive.

For real fail-operational safety, these safeguarding concepts must be complemented by an active safety component capable of providing a feasible fallback solution [4]. A promising direction is to execute a lightweight trajectory planner on an independent, real-time platform, called Safety Island [6]. This

K. Moller, G. Tungka, L. Jürgens and J. Betz are with the Professorship of Autonomous Vehicle Systems, TUM School of Engineering and Design, Technical University of Munich, 85748 Garching, Germany; Munich Institute of Robotics and Machine Intelligence (MIRMI).

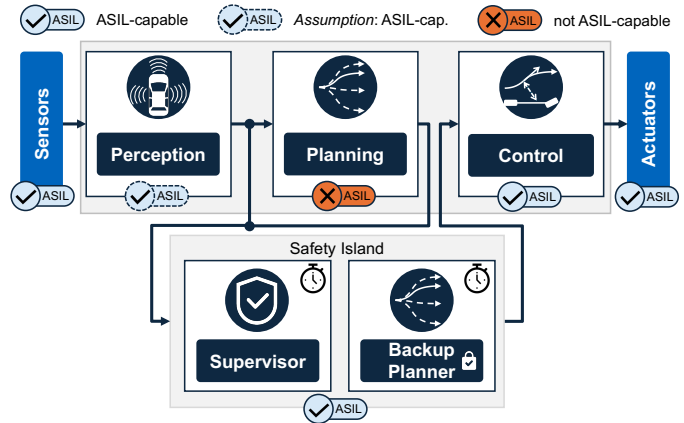


Fig. 1. System architecture illustrating the integration of a safety island that hosts both a Supervisor and an embedded planner. The concept enables safety monitoring and fallback trajectory generation independently of the main software stack, forming the foundation for fail-operational AD.

planner should continuously generate fallback trajectories that the control stack uses in case of a failure. Compared to a fully redundant system on a second high-performance unit, this approach offers a cost-efficient and resource-aware path for active safety systems.

The long-term objective of this research is to integrate such an embedded backup planner as an active extension to an existing safeguarding framework. While the envisioned system will eventually run in parallel with the main planning module, this work represents an important first step toward that goal. We demonstrate the feasibility of deploying a sampling-based trajectory planner [7] on an automotive-grade, embedded platform running a Real-Time Operating System (RTOS). The focus lies on achieving deterministic timing and reliable computation under constrained resources, thereby quantifying both the potential and the limitations of real-time planning on safety-certifiable hardware. An overview of the envisioned architecture is shown in Figure 1. The main contributions of this paper are as follows:

- A safety-oriented planning concept that can extend runtime safeguarding by introducing a fallback mechanism for fail-operational AD.
- An embedded real-time implementation of a sampling-based trajectory planner optimized for deterministic execution under limited resources.
- An empirical evaluation of latency, jitter, and CPU utilization, providing insight into the feasibility and challenges of deploying active safety logic on constrained hardware.

II. RELATED WORK

In the context of AD, motion planning is not only a question of correctness but also of timing. A motion planner must produce safe and feasible trajectories, yet the computation time itself becomes a constraint: results are only useful if they are available before a strict deadline. This requirement is a major concern of real-time computing, where the decisive criterion is not only high throughput or performance, but the guarantee that a task completes reliably within its allocated time window [8]. For AVs, this means that planning algorithms must balance responsiveness and fidelity with deterministic execution, even when running under constrained resources. In recent years, several planning concepts have been developed [9]. These methods can be categorized into optimization-, graph-, sampling-, and machine learning-based algorithms [10]. Every class offers specific trade-offs in terms of runtime or predictability properties.

Optimization-based methods formulate motion planning as a constrained optimization problem, in which a cost function is minimized subject to vehicle dynamics, actuator limitations, and environmental constraints [11], [12]. Approaches such as Quadratic Programming and Model Predictive Control (MPC) [13] optimize trajectories by calculating future system states and guaranteeing feasibility at each step. These methods yield smooth and consistent motion profiles and allow the explicit incorporation of safety-relevant constraints. However, their computational demand is considerable, especially in dynamic environments, where repeated online optimization becomes a bottleneck. Direct optimal-control formulations [14] further improve accuracy but still face challenges regarding runtime, memory consumption, and predictable execution.

Graph-based methods discretize the planning space into nodes and edges, enabling the use of established search algorithms such as A* [15]. They are especially effective in structured environments [16], where a sufficiently fine grid guarantees that a drivable path can be found if one exists. Nevertheless, high spatial resolution quickly increases computational requirements, and the resulting paths often need smoothing before they can be executed by a vehicle [17]. Moreover, classic graph-based planners operate in the spatial domain and therefore do not handle dynamic obstacles well. To incorporate temporal information, extensions such as spatiotemporal graphs [18], [19] augment the graph structure with velocity and timing profiles, yielding full spatiotemporal trajectories at the cost of additional computational effort.

Sampling-based methods compute a finite set of trajectory candidates by sampling in the action or control space around the current Ego Vehicle (EV) state [7], [20], [21]. Each candidate is evaluated with respect to feasibility constraints, such as curvature or acceleration and ranked using cost functions that capture safety, comfort, and efficiency [17]. The computational load can be adjusted by varying the number of samples, making these methods particularly suitable for real-time applications where predictable runtime is essential.

However, planning quality depends on sampling density and coverage [7]: insufficient sampling may miss feasible or desirable maneuvers, while excessive sampling increases runtime. Despite these limitations, sampling-based planners remain a widely used approach between expressiveness, robustness, and computational tractability.

III. METHODOLOGY

While numerous motion planning frameworks have been proposed to achieve real-time capability in AD [2], [22], [23], most implementations operate on High-Performance Computers (HPCs) using general-purpose operating systems. These environments provide large computational resources but lack deterministic scheduling and guaranteed timing behavior. This work, therefore, investigates the deployment of a motion planner on an embedded platform running an RTOS. The RTOS provides preemptive scheduling of tasks, bounded interrupt latency, and a low-footprint execution environment, enabling the implementation of applications satisfying hard real-time requirements under constrained compute power. The presented system represents a fully functional planning stack, operating as the primary decision-making component within an AD architecture. It interacts with perception, localization, and control subsystems through communication interfaces. The system overview is shown in Figure 2.

A. Prerequisites and Assumptions

Our motion planner assumes input information is provided by the AD stack. At each planning step t , the planner requires the current EV state \mathbf{x}_t in cartesian coordinates,

$$\mathbf{x}_t = (x_t, y_t, v_t, a_t, \theta_t)^\top, \quad (1)$$

where (x_t, y_t) denote the EV position in the world frame, v_t , a_t and θ_t represent the current velocity, acceleration and orientation, respectively. The EV state is assumed to be estimated by a localization module.

Our motion planner further needs a geometrically valid reference path Γ , defined as a continuously differentiable curve

$$\Gamma = \{(x_r(s), y_r(s), \theta_r(s)) \mid s \in [0, S]\}, \quad (2)$$

which provides a reference for local trajectory planning. To maintain a bijective mapping between cartesian and curvilinear coordinates, Γ has to be non-self-intersecting and to exhibit bounded curvature $|\kappa_r(s)| < \kappa_{\max}$ for all $s \in [0, S]$. This ensures that every cartesian point in the projection domain along Γ can be transformed to a unique longitudinal coordinate s and lateral coordinate d .

In addition to Γ , the environment contains a finite set of objects

$$\mathcal{O}_t = \{o_t^1, o_t^2, \dots, o_t^M\}, \quad (3)$$

where each object o_t^j is characterized by a predicted trajectory over a finite horizon, provided by an upstream perception and prediction module.

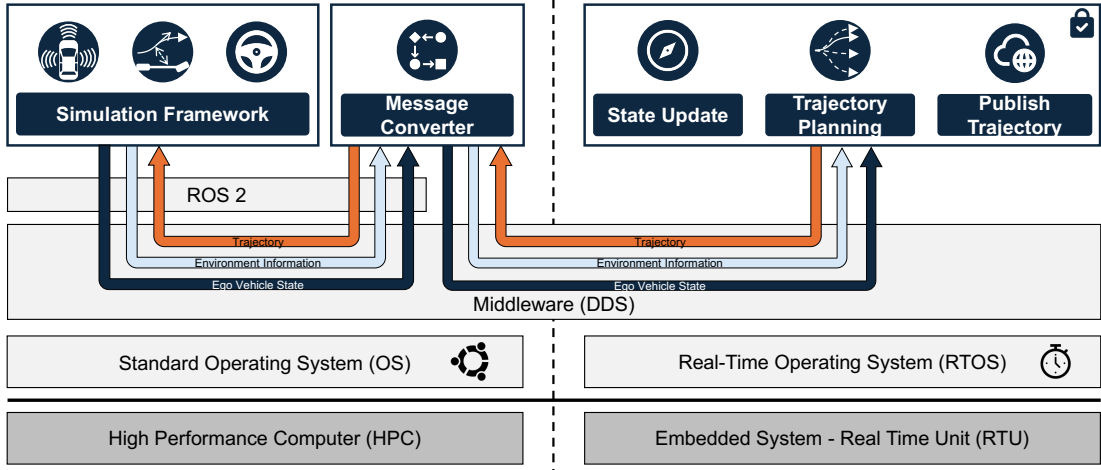


Fig. 2. Overview of the proposed communication architecture between the HPC and the Embedded System. The HPC runs a ROS 2 simulation, while the RTOS executes our motion planner. A lightweight DDS bridge enables data exchange across both platforms.

The planner’s output at each cycle is a single trajectory ξ_t , represented as a discrete sequence of states over a finite horizon τ with uniform time increment Δt :

$$\xi_t = \{\mathbf{x}_0, \mathbf{x}_1, \dots, \mathbf{x}_N\}. \quad (4)$$

Each state of ξ_t , as described in Equation 1, corresponds to the planned vehicle motion at time $t + i\Delta t$. The trajectory serves as input for a downstream control module that executes the trajectory and compensates for external disturbances.

B. Communication Interface

Current robotics or AD applications such as Autoware¹ or high-performance autonomous racing stacks [24] often rely on ROS 2 as middleware due to its modular architecture and broad ecosystem support. Despite its flexibility, ROS 2 is not designed for hard real-time operation, as its message-passing concept introduces nondeterministic scheduling and dynamic memory allocation overheads [25]. Due to the high coupling of ROS 2 to Linux, including its dependencies, e.g., Python or a file system, ROS 2 applications cannot be ported directly to RTOS like Zephyr². However, multiple Data Distribution Service (DDS) clients or micro-ROS implementations are available to enable data exchange between different systems. In this work, communication between the high-performance domain and the embedded planner is realized through a minimal DDS bridge. The high-performance node, running the ROS-based software stack, publishes the EV-state \mathbf{x}_t , reference path Γ , and surrounding obstacles \mathcal{O}_t , which are translated into DDS messages and sent to the RTOS domain [4]. The embedded planner subscribes to these DDS topics, performs motion planning, and returns the resulting trajectory through the same interface. This design maintains full compatibility with ROS 2-based systems without the need to run a complete ROS 2 runtime on the embedded platform.

¹<https://autoware.org/>

²<https://www.zephyrproject.org/>

C. Execution Workflow on the Embedded Platform

Our motion planner is executed as a standalone module on the embedded platform and follows a cyclic workflow, as shown in Figure 3.

Each planning cycle begins with the initialization stage, where the system configures its network connection, starts the DDS client and initializes the motion planner. It also processes the reference path and creates the curvilinear coordinate system. This setup is performed once at startup and remains static during runtime.

During the online phase, the planner iteratively performs four steps. First, the current EV state \mathbf{x}_t is received via the DDS interface and stored in shared memory accessible to the planning thread. Second, the planner generates candidate trajectories $\xi \in \mathcal{T}$ based on predefined sampling parameters. Third, each trajectory is evaluated according to feasibility and basic cost metrics, as detailed in the following section. Finally, the selected trajectory ξ^* is serialized and transmitted back to the HPC. The cycle repeats continuously until the scenario goal is reached or the execution is terminated.

D. Trajectory Generation and Evaluation

The trajectory generation process follows a sampling-based approach formulated in the curvilinear frame (s, d) , which expresses vehicle motion relative to the global reference path Γ [20]. A candidate trajectory $\xi : [0, \tau] \rightarrow \mathbb{R}^m$ is defined by the mapping

$$\xi = \mathcal{P}(\mathbf{x}(0), g(\tau), \Gamma), \quad (5)$$

where $g(\tau)$ represents the sampled goal state at the end of the planning horizon τ .

Following the formulation in [7], [20], longitudinal movement is represented by a quartic polynomial

$$s(t) = a_0 + a_1t + a_2t^2 + a_3t^3 + a_4t^4, \quad (6)$$

and the lateral motion by a quintic polynomial

$$d(t) = b_0 + b_1t + b_2t^2 + b_3t^3 + b_4t^4 + b_5t^5. \quad (7)$$

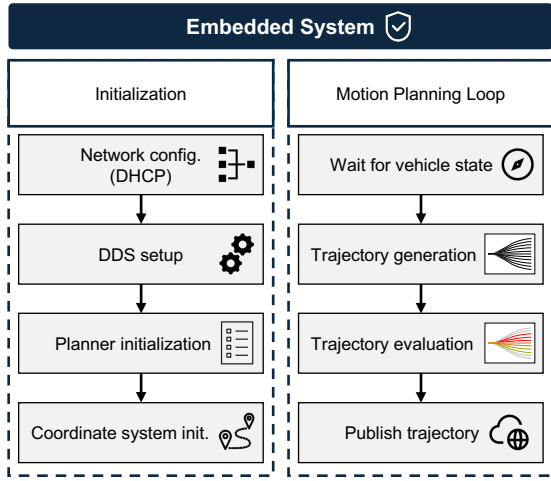


Fig. 3. Overview of the planning workflow on the embedded platform. The initialization phase (left) is executed once at startup, followed by the cyclic motion planning loop (right).

The polynomial coefficients are analytically calculated from the boundary conditions created by the initial state $\mathbf{x}(0)$ and $g(\tau)$. For the lateral component, the goal velocity and acceleration are set to zero to ensure that the EV aligns with Γ at the end of each trajectory sample [20]. This formulation minimizes jerk while maintaining low computational complexity.

Our planner generates a discrete set of goal states $g_k(\tau)$ by sampling time, lateral offset, and goal velocity, following the approach described in [7]. The sampling ranges are defined as

$$\tau \in [\tau_{\min}, \tau_{\max}], d_{\tau} \in [d_{\min}, d_{\max}], v_{\tau} \in [v_{\min}, v_{\max}], \quad (8)$$

where each set $(\tau, d_{\tau}, v_{\tau})$ yields one candidate trajectory ξ . By combining m longitudinal and n lateral samples, a set of $m \times n$ candidate trajectories is created. Each trajectory is transformed back into cartesian coordinates using the curvilinear projection along Γ [20].

All trajectory candidates are then evaluated for kinematic feasibility according to the vehicle's physical limits. The longitudinal acceleration must satisfy

$$a_{\min} \leq a(t) \leq a_{\max}(t), \quad \forall t \in [t_0, \tau], \quad (9)$$

and the curvature $\kappa(t)$ must remain below the limit created by the maximum steering angle δ_{\max} and wheelbase L :

$$|\kappa(t)| \leq \frac{\tan(\delta_{\max})}{L}, \quad \forall t \in [t_0, \tau]. \quad (10)$$

Additional constraints apply to the rate of curvature change and the yaw rate:

$$|\dot{\kappa}(t)| \leq \dot{\kappa}_{\max}, \quad \forall t \in [t_0, \tau], \quad (11)$$

$$|\dot{\psi}(t)| \leq \kappa_{\max} \cdot v(t), \quad \forall t \in [t_0, \tau]. \quad (12)$$

Trajectories that violate any of these limits are discarded before being evaluated for cost, thereby reducing runtime.

The feasible trajectories are finally ranked according to a cost function that combines multiple comfort and safety

criteria [7]. Representative examples include the lateral deviation from Γ ,

$$J_{\text{ref}}(\xi) = \sum_{i=0}^N (d_i^{\perp})^2, \quad (13)$$

the velocity offset with respect to a desired speed v_{des} ,

$$J_{\text{vel}}(\xi) = \sum_{i=0}^N |v_i - v_{\text{des}}|^p, \quad (14)$$

and acceleration-based measures,

$$J_{\text{lat}}(\xi) = \int_{t_0}^{\tau} a_{\text{lat}}(t)^2 dt, \quad J_{\text{lon}}(\xi) = \int_{t_0}^{\tau} a_{\text{lon}}(t)^2 dt. \quad (15)$$

The total trajectory cost is calculated as a weighted sum

$$J_{\text{sum}}(\xi) = \sum_{i=1}^n \omega_i J_i(\xi), \quad (16)$$

where ω_i are the corresponding weighting factors. The optimal trajectory is selected as

$$\xi^* = \arg \min_{\xi \in \mathcal{T}_{\text{feas}}} (J_{\text{sum}}(\xi)). \quad (17)$$

Executing this planning algorithm on Zephyr RTOS with limited hardware resources introduces additional challenges that influence the implementation. Zephyr provides a lightweight runtime optimized for deterministic task scheduling, but it lacks full support for the C++ standard library. Consequently, several libraries commonly used in motion planning algorithms, such as Boost, are unavailable. Geometric operations required for feasibility checks, including polygon intersection and point-in-polygon tests, are therefore substituted using the lightweight Clipper2 library.

IV. RESULTS & DISCUSSION

The following section presents the experimental evaluation of our proposed real-time motion planner, which is executed on the embedded platform under the Zephyr RTOS. The objective of this study is to evaluate the computational performance of our planning algorithm under constrained hardware conditions and to derive insights for future extensions toward fail-operational planning architectures.

The following evaluation focuses on runtime characteristics, e.g., latency, jitter, and CPU utilization. In addition, qualitative analyses are conducted to verify that the planning process preserves the expected planning behavior compared to the reference implementation [7].

A. Experimental Setup

All experiments were conducted on an automotive-grade embedded platform based on the NXP[®] S32Z2 real-time processor. The system uses an Arm[®] Cortex-R52 core running at 800 MHz under Zephyr RTOS (v3.5). In our evaluation setup, the HPC corresponds to a desktop system with 16 logical processors, 32 GB RAM, and a base frequency of 2.2 GHz running Ubuntu 22.04. The HPC executes an adapted CommonRoad environment [26], enabling a reproducible

ROS 2-based evaluation of our planning framework. In all experiments, each trajectory was parameterized over a fixed horizon of 30 time steps with a resolution of $\Delta t = 0.1$ s. To isolate baseline timing behavior, no obstacles were considered during this evaluation. Each trajectory batch was visualized and checked for consistency.

B. Qualitative Evaluation

For qualitative validation, we executed a standard CommonRoad [26] scenario, in which the EV must perform a left turn at an unsignalized intersection, as shown in Figure 4. This scenario enables a thorough analysis of feasibility and cost calculation mechanisms, as well as verification of the cartesian-to-curvilinear projection. The generated trajectories are aligned with the lane boundaries, and both feasibility and cost evaluation yield consistent results within the CommonRoad simulation framework.

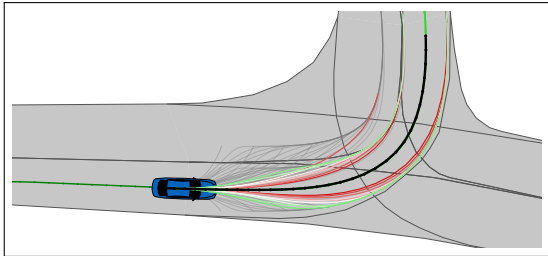


Fig. 4. Qualitative simulation result in the CommonRoad environment, showing a left-turn scenario at an unsignalized intersection. The generated candidate trajectories follow the reference path, illustrating how the planner maintains smooth motion during the intended turning maneuver.

Figure 5 furthermore details the set of generated trajectory candidates, shown in both curvilinear (Figure 5a) and cartesian (Figure 5b) coordinates. Each line represents one trajectory candidate ξ , where infeasible trajectories are drawn in gray and feasible ones are color-coded according to their total cost, ranging from green (low cost) to red (high cost). The optimal trajectory ξ^* is selected based on the overall cost function (Equation 17) and is shown in black.

As introduced in Section III-D, the sampling parameters directly influence the generated trajectory tree. Lateral offsets correspond to different displacements, while variations in goal velocity and time horizon affect the goal states in both position and timing. Figure 5 visualizes how these sampling parameters influence the shape and density of all generated trajectories \mathcal{T} . It also provides a representation of the planner’s evaluation logic, allowing for validation of its feasibility and cost calculation pipeline. Trajectories with high lateral offset from Γ or large longitudinal acceleration are penalized through corresponding cost terms. Likewise, deviations from a desired cruise speed increase the total cost. No parameter tuning was done for this example; all weighting factors were selected manually, and the desired velocity was fixed to $7.0 \frac{\text{m}}{\text{s}}$ for illustrative purposes only. While this visualization shows the evaluation of all trajectory candidates, a real-world deployment would only publish the optimal trajectory to the controller.

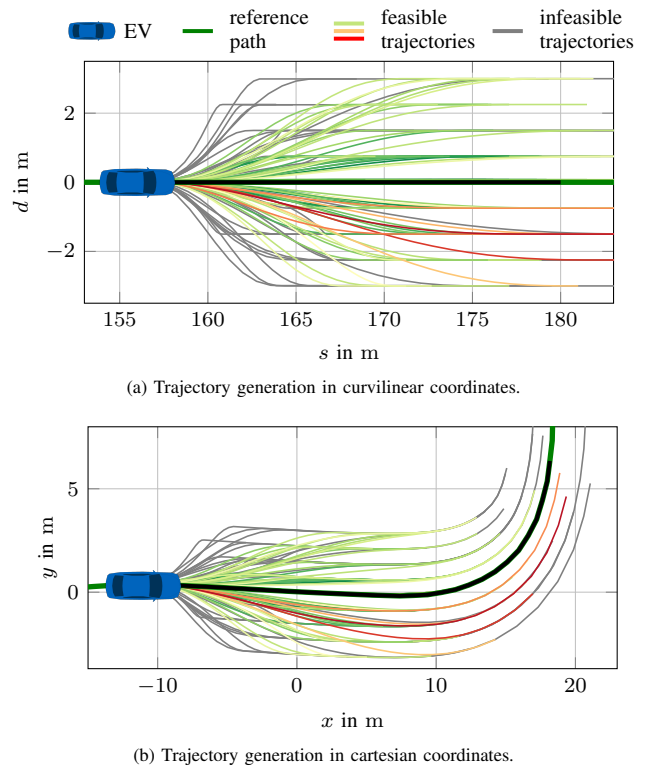


Fig. 5. Generation and evaluation of trajectory samples by the planner along Γ . Valid trajectories are color-coded based on their cost, ranging from green (low cost) to red (high cost). The optimal trajectory is shown in black.

C. Runtime and Latency Evaluation

To analyze the temporal behavior of our embedded planner, three metrics are evaluated: the average runtime T_{avg} , the worst-case runtime T_{max} , and the jitter J . These are defined in the following equations, where T_i denotes the runtime of the i -th planning cycle and n the total number of iterations.

$$T_{\text{avg}} = \frac{1}{n} \sum_{i=1}^n T_i \quad (18)$$

$$T_{\text{max}} = \max(T_i) \quad (19)$$

$$J = \max(|T_i - T_{\text{avg}}|) \quad (20)$$

To compare the latency characteristics of the embedded platform with those of a regular HPC, both systems were configured to execute the same planning task, consisting of 64 trajectory samples per cycle. On the HPC, three configurations were tested: an idle setup without background load, a setup with the Autoware stack running concurrently, and a setup with synthetic load introduced on 8 of 16 cores. Figure 6 illustrates the measured runtimes of consecutive planning cycles for both systems.

As expected, the HPC achieves lower average runtimes due to its higher processing power. However, under concurrent execution, significant temporal variability can be observed. When the background system load increases, the runtime distribution widens, and latency peaks occur as a consequence

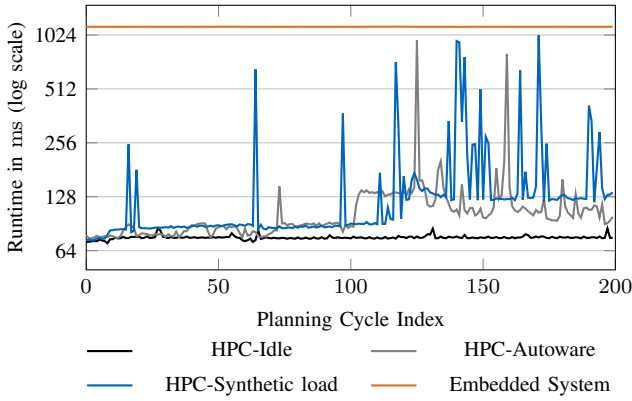


Fig. 6. Comparison of runtime behavior between the embedded RTOS-based platform and the HPC under varying computational load. The embedded board exhibits stable timing behavior with minimal jitter.

of process preemption and interference within the Linux scheduler. In contrast, our embedded platform running the RTOS maintains stable execution with a mean runtime of approximately 1138 ms and negligible jitter across all measurements.

This comparison highlights a fundamental difference between high-performance and real-time systems. While Linux-based environments can, in principle, achieve real-time behavior through kernel-level tuning, adapted scheduling, and CPU pinning, such configurations require high engineering effort and are sensitive to kernel version, driver behavior, and system load. Ensuring deterministic behavior in such environments requires careful selection of the scheduler, strict control of thread priorities, and pre-allocating memory pages to prevent blocking operations. Even then, effects such as cache pollution or non-preemptive kernel modules (e.g., GPU drivers) can compromise timing predictability.

In contrast, our Zephyr-based setup provides a deterministic execution environment by design. The RTOS enables bounded interrupt latency, fixed-priority scheduling, and complete control over memory allocation. Consequently, the runtime characteristics remain unaffected by external processes or concurrent tasks, making it a more reliable platform for safety-critical applications. From a system design perspective, this determinism enables a robust separation of safety domains. A complex AV software stack may operate on the HPC, while the RTOS executes on the embedded platform. This architectural separation offers a path toward ASIL-compliant implementations, where the planner serves as a safety function operating independently of the main software stack.

To further analyze runtime behavior, the planner was executed with increasing numbers of trajectory samples (16, 32, 64, and 100). For 16 samples, the total runtime is around 287 ms, increasing to approximately 1.78 s for 100 samples. Despite the limited computational resources, the board maintains a low jitter across all configurations, confirming deterministic execution. At lower sample counts, the system operates within real-time bounds, sustaining a planning frequency of roughly 2 Hz.

This behavior shows the trade-off between trajectory diversity and computation time. Increasing the number of samples enhances coverage of the solution space and may yield smoother or safer trajectories, but comes at the cost of increased computation time. Table I summarizes the results for 16, 32, 64, and 100 trajectories.

TABLE I
TIMING METRICS FOR DIFFERENT NUMBERS OF TRAJECTORY SAMPLES ON THE EMBEDDED SYSTEM.

Metric	Trajectories			
	16	32	64	100
Min. runtime (ms)	287.42	570.37	1137.39	1774.45
Max. runtime (ms)	287.83	570.68	1138.96	1777.48
Avg. runtime (ms)	287.67	570.49	1138.00	1775.22
Jitter (ms)	0.41	0.31	1.57	3.03
Jitter (%)	0.14	0.05	0.14	0.17
Avg. time / trajectory (ms)	17.98	17.83	17.78	17.75

The total runtime increases linearly with the number of trajectories. The average computation time per trajectory remains nearly constant at around 17.8 ms, indicating that no additional overhead occurs as the workload increases. The observed jitter values are consistently around or below 3 ms, corresponding to less than 0.2% of the total runtime. This high level of determinism is further supported by the results shown in Figure 7. The boxplot illustrates four independent

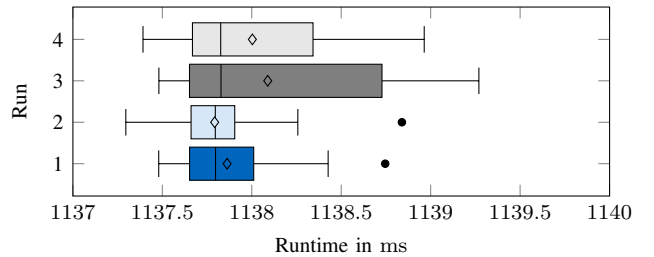


Fig. 7. Measured runtime distribution of the embedded planner for four independent runs (500 iterations, each 64 trajectories). The results demonstrate highly deterministic execution with sub-millisecond jitter.

runs, each comprising 500 planning cycles with 64 trajectories per cycle. Across all four runs, the execution time fluctuates only within a millisecond range, confirming that the RTOS provides reproducible timing over extended periods.

Figure 8 shows the breakdown of total runtime into trajectory generation and evaluation stages, along with the corresponding CPU utilization. The evaluation accounts for the majority of the total computation time. This phase involves converting polynomial coefficients into discrete trajectory points, transforming coordinates from curvilinear to cartesian space, and evaluating feasibility and cost for all trajectories. These operations dominate the runtime and CPU usage, indicating that this stage provides great potential for optimization. While the absolute runtime is not yet sufficient for a primary motion planner, the achieved determinism and bounded latency make the proposed approach suitable as a backup or safety planner within a fail-operational system, as

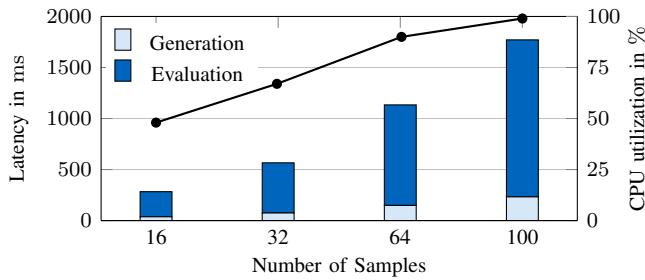


Fig. 8. Runtime breakdown and CPU utilization for different sample counts. The black line corresponds to the CPU utilization shown on the right y-axis.

motivated in Figure 1. In this use case, trajectories could be generated in the background and be activated when the main planner fails. Moreover, the results underline the importance of advanced sampling strategies. In the current implementation, samples are distributed uniformly across the action space, resulting in trajectory evaluations in irrelevant regions. Informed sampling approaches could concentrate computational effort on important subsets of the action space, for instance. This would reduce computational load without compromising the coverage of feasible trajectories.

V. CONCLUSION & OUTLOOK

This work presented the implementation and evaluation of a sampling-based motion planner executed on automotive-grade embedded hardware under real-time operating conditions. The planner was deployed on an Arm-based NXP S32Z2 platform running Zephyr RTOS and evaluated using the CommonRoad simulation framework. The results demonstrate that deterministic trajectory planning is feasible on constrained embedded systems, with constant execution times and minimal jitter. Although the absolute runtime is higher than that of an HPC, the embedded solution shows better timing consistency and predictability. These characteristics are critical for safety-certified applications, where deterministic response behavior is more important than peak computational speed. Our presented concept, therefore, provides a promising foundation for a certified fallback planner that operates independently of the main AD stack.

Future work will focus on transferring the concept into a comprehensive safety architecture, where the planner acts as a Minimal Risk Maneuver (MRM) module capable of generating trajectories in the event of a primary system failure. Furthermore, the concept will be validated on a real vehicle to evaluate its robustness under real-world conditions.

REFERENCES

- [1] I. Nastjuk, B. Herrenkind, M. Marrone, A. B. Brendel, and L. M. Kolbe, "What drives the acceptance of autonomous driving? An investigation of acceptance factors from an end-user's perspective," *Technological Forecasting and Social Change*, 2020.
- [2] M. D. Tezerjani, D. Qu, S. Dhakal, D. Carrillo, A. Mirzaeina, and Q. Yang, *Real-Time Motion Planning for Autonomous Vehicles in Dynamic Environments*. Springer Nature Switzerland, 2025.
- [3] T. Stahl, M. Eicher, J. Betz, and F. Diermeyer, "Online Verification Concept for Autonomous Vehicles – Illustrative Study for a Trajectory Planning Module," in *2020 IEEE 23rd International Conference on Intelligent Transportation Systems (ITSC)*. IEEE, 2020.
- [4] K. Moller, R. Neher, M. Seegert, and J. Betz, "Towards Safe Autonomous Driving: A Real-Time Safeguarding Concept for Motion Planning Algorithms," in *2025 IEEE International Conference on Vehicular Electronics and Safety (ICVES)*. IEEE, 2025, accepted.
- [5] International Organization for Standardization, "ISO 26262:2018 Road vehicles – Functional safety," Geneva, Switzerland, 2018.
- [6] arm. (2025) Implement safety-critical isolation using safety island architecture. Accessed: 2025-11-13. [Online]. Available: https://learn.arm.com/learning-paths/automotive/openadkit2_safetyisolation/1d_safety_island_arch
- [7] R. Trauth, K. Moller, G. Würsching, and J. Betz, "FRENEX: A High-Performance and Modular Motion Planning Framework for Autonomous Driving," *IEEE Access*, 2024.
- [8] G. Buttazzo, *Hard Real-Time Computing Systems: Predictable Scheduling Algorithms and Applications*. Springer Nature, 2024.
- [9] S. Teng, X. Hu, P. Deng, B. Li, Y. Li, Y. Ai, D. Yang *et al.*, "Motion Planning for Autonomous Driving: The State of the Art and Future Perspectives," *IEEE Transactions on Intelligent Vehicles*, 2023.
- [10] J. Hu, Y. Wang, S. Cheng, J. Xu, N. Wang, B. Fu, Z. Ning *et al.*, "A survey of decision-making and planning methods for self-driving vehicles," *Frontiers in Neurobotics*, 2025.
- [11] Y. Li, "Motion Planning for Dynamic Scenario Vehicles in Autonomous-Driving Simulations," *IEEE Access*, 2023.
- [12] Z. Arjmandzadeh, M. H. Abbasi, H. Wang, J. Zhang, and B. Xu, "A Lyapunov Optimization-Based Approach to Autonomous Vehicle Local Path Planning," *Sensors*, 2024.
- [13] C. Liu, S. Lee, S. Varnhagen, and H. E. Tseng, "Path planning for autonomous vehicles using model predictive control," in *2017 IEEE Intelligent Vehicles Symposium (IV)*. IEEE, 2017.
- [14] S. Luo, X. Li, and Z. Sun, "An Optimization-based Motion Planning Method for Autonomous Driving Vehicle," in *2020 3rd International Conference on Unmanned Systems (ICUS)*. IEEE, 2020.
- [15] P. Hart, N. Nilsson, and B. Raphael, "A Formal Basis for the Heuristic Determination of Minimum Cost Paths," *IEEE Transactions on Systems Science and Cybernetics*, 1968.
- [16] D. Dolgov, S. Thrun, M. Montemarlo, and J. Diebel, "Path Planning for Autonomous Vehicles in Unknown Semi-structured Environments," *The International Journal of Robotics Research*, 2010.
- [17] J. Huang, Z. He, Y. Arakawa, and B. Dawton, "Trajectory Planning in Frenet Frame via Multi-Objective Optimization," *IEEE Access*, 2023.
- [18] Y. Shu, J. Zhou, and F. Zhang, "Agile Decision-Making and Safety-Critical Motion Planning for Emergency Autonomous Vehicles," *IEEE Transactions on Intelligent Transportation Systems*, 2025.
- [19] M. Rowold, L. Ögretmen, T. Kerbl, and B. Lohmann, "Efficient Spatiotemporal Graph Search for Local Trajectory Planning on Oval Race Tracks," *Actuators*, 2022.
- [20] M. Werling, J. Ziegler, S. Kammel, and S. Thrun, "Optimal trajectory generation for dynamic street scenarios in a Frenet Frame," in *2010 IEEE International Conference on Robotics and Automation*, 2010.
- [21] M. Kim, A. Esquerre-Pourtère, and J. Park, "Robust Real-Time Sampling-Based Motion Planner for Autonomous Vehicles in Narrow Environments," *IEEE Transactions on Automation Science and Engineering*, 2025.
- [22] J. Cheng, Y. Chen, Q. Zhang, L. Gan, C. Liu, and M. Liu, "Real-Time Trajectory Planning for Autonomous Driving with Gaussian Process and Incremental Refinement," in *2022 International Conference on Robotics and Automation (ICRA)*. IEEE, 2022.
- [23] W. Xu, J. Wei, J. M. Dolan, H. Zhao, and H. Zha, "A real-time motion planner with trajectory optimization for autonomous vehicles," in *IEEE International Conference on Robotics and Automation*. IEEE, 2012.
- [24] J. Betz, T. Betz, F. Fent, M. Geisslinger, A. Heilmeyer, L. Hermansdorfer, T. Herrmann *et al.*, "TUM autonomous motorsport: An autonomous racing software for the Indy Autonomous Challenge," *Journal of Field Robotics*, 2023.
- [25] H. Teper, O. Bell, M. Günzel, C. Gill, and J.-J. Chen, "Reconciling ROS 2 with Classical Real-Time Scheduling of Periodic Tasks," in *2025 IEEE 31st Real-Time and Embedded Technology and Applications Symposium (RTAS)*. IEEE, 2025.
- [26] M. Althoff, M. Koschi, and S. Manziinger, "CommonRoad: Composable benchmarks for motion planning on roads," in *IEEE Intelligent Vehicles Symposium*, 2017.